Quantitative cerebral H$_2$^{15}O perfusion PET without arterial blood sampling, a method based on washout rate

Valerie Treyer, Mathieu Jobin, Cyrill Burger, Vincenzo Teneggi, Alfred Buck

PET Center, Division of Nuclear Medicine, University Hospital Zurich, Zurich, Switzerland, GlaxoSmithKline Medicine Research Centre, Verona, Italy

Abstract. The quantitative determination of regional cerebral blood flow (rCBF) is important in certain clinical and research applications. The disadvantage of most quantitative methods using H$_2$^{15}O positron emission tomography (PET) is the need for arterial blood sampling. In this study a new non-invasive method for rCBF quantification was evaluated. The method is based on the washout rate of H$_2$^{15}O following intravenous injection. All results were obtained with Alpert's method, which yields maps of the washin parameter K_1 (rCBF$_{K1}$) and the washout parameter k_2 (rCBF$_{k2}$). Maps of rCBF$_{K1}$ were computed with measured arterial input curves. Maps of rCBF$_{k2*}$ were calculated with a standard input curve which was the mean of eight individual input curves. The mean of grey matter rCBF$_{k2*}$ (CBF$_{k2*}$) was then compared with the mean of rCBF$_{K1}$ (CBF$_{K1}$) in ten healthy volunteer smokers who underwent two PET sessions on day 1 and day 3. Each session consisted of three serial H$_2$^{15}O scans. Reproducibility was analysed using the rCBF difference scan 3–scan 2 in each session. The perfusion reserve (PR=rCBF$_{acetazolamide}$–rCBF$_{baseline}$) following acetazolamide challenge was calculated with rCBF$_{k2*}$ (PR$_{k2*}$) and rCBF$_{K1}$ (PR$_{K1}$) in ten patients with cerebrovascular disease. The difference CBF$_{k2*}$–CBF$_{K1}$ was 5.90±8.12 ml/min/100 ml (mean±SD, n=55). The SD of the scan 3–scan 1 difference was 6.1% for rCBF$_{k2*}$ and rCBF$_{K1}$, demonstrating a high reproducibility. Perfusion reserve values determined with rCBF$_{K1}$ and rCBF$_{k2*}$ were in high agreement (difference PR$_{k2*}$–PR$_{K1}$=−6.5±10.4%, PR expressed in percentage increase from baseline). In conclusion, a new non-invasive method for the quantitative determination of rCBF is presented. The method is in good agreement with Alpert's original method and the reproducibility is high. It does not require arterial blood sampling, yields quantitative voxel-by-voxel maps of rCBF, and is computationally efficient and easy to implement.

Alfred Buck (✉)
PET Center, Division of Nuclear Medicine,
University Hospital Zurich, Rämistrasse 100,
8091 Zurich, Switzerland
e-mail: buck@nuklearmed.unizh.ch
Tel.: +41-1-2553547, Fax: +41-1-2554414

Introduction

The quantitative determination of regional cerebral blood flow (rCBF) has clinical and research applications. The evaluation of rCBF is important in patients in whom a cerebral revascularisation procedure such as endarterectomy or extra-intracranial bypass surgery is planned [1, 2, 3, 4]. An often-used parameter to identify areas with compromised rCBF is the perfusion reserve, which is defined as the increase in rCBF following vasodilatation. The latter can be induced by the application of CO$_2$-enriched breathing air or the intravenous administration of acetazolamide. While a qualitative evaluation of rCBF is often sufficient, there are instances where a fully quantitative assessment is advantageous. For example, if one wants to evaluate the effect of a drug on rCBF, qualitative imaging would miss global effects. Several methods have been proposed for the quantitative assessment of rCBF using H$_2$^{15}O positron emission tomography (PET). A commonly used one based on weighted integration was developed by Alpert et al. [5]. Other methods use the autoradiographic approach [6, 7]. All of these methods require knowledge of the arterial tracer concentration (input curve), which can be obtained by cannulation of the radial artery. This is impractical in a clinical setting. There is therefore a clear need for non-invasive methods. One such method was introduced by Watabe et al. [8]. At its core is the assessment of a high-flow and a low-flow region under the assumption that the input curve is the same. Another method allowing the quantifi-

cation of rCBF changes was developed by Fox et al. [9]. We presented a method based on the assessment of the accumulated $H_2^{15}O$ activity over the first 60 s normalised to injected activity. It proved to be useful for the quantitative evaluation of the perfusion reserve, but not for rCBF per se [10]. In the present work we evaluated another alternative which is based on Alpert's method. In contrast to the original method, quantification is derived from the washout parameter k_2, which is dependent on the shape and not the scale of the input curve. The method is non-invasive, yields quantitative maps of rCBF and is computationally efficient and easy to implement. The reproducibility was assessed in a volunteer group who had serial scans. The absolute values were compared with Alpert's original method as gold standard and with Watabe's method. Furthermore, the suitability for assessment of perfusion reserve using acetazolamide challenge was evaluated in a patient group.

Materials and methods

Volunteers

Ten healthy male volunteers were taken from a control group of a pharmacological study. They were chronic smokers, aged 44.1±7.6 years (mean±SD, range 35–61). The subjects were hospitalised for 4 days. PET sessions took place on day 1 and day 3. Each consisted of three successive rCBF measurements at 10-min intervals.

Patients

The patient group comprised ten subjects. All were referred to PET for the preoperative evaluation of rCBF. Five patients suffered from stenoses in either the carotid or the vertebral arteries (two males, 44 and 60 years, and three females, 57, 63 and 73 years). Three patients had moyamoya disease [11] (two males, one female, aged 2, 6 and 5 years). One 29-year-old had a frontal arteriovenous malformation and one 44-year-old male suffered from a haemangiopericytoma.

$H_2^{15}O$ PET

Volunteers. The imaging protocol involved two scanning sessions, one on day 1 and one on day 3. Both sessions took place between 4 and 6 p.m. Each session consisted of three serial rCBF measurements with a 10-min decay interval in between. A total of 60 rCBF measurements were acquired, 55 of which could be analysed; in five the arterial input curve (AIC_m) was not available due to clogging of the radial catheter.

Patients. A total of two rCBF measurements was performed in each patient, one at baseline and one 13 min following the intravenous administration of 1 g acetazolamide. In the children the acetazolamide dose was adjusted according to weight.

The PET studies were performed in 3-D mode on a whole-body scanner (Advance, GE Medical Systems, Milwaukee, Wis., USA). This is a scanner with an axial field of view of 14.6 cm and a reconstructed in-plane resolution of 7 mm. Prior to positioning of the patients in the scanner, catheters were placed in an antecubital vein for tracer injection and the radial artery for blood sampling. For each PET measurement, 400–800 MBq $H_2^{15}O$ was injected intravenously using an automatic injection device which delivers a predefined dose of $H_2^{15}O$ over 20 s. Following the arrival of the bolus in the brain, a series of 18 10-s scans was initiated. The scans were corrected for photon attenuation using a 10-min germanium-68 transmission scan. The time course of the arterial radioactivity was assessed by continuous sampling of blood drawn from the radial artery, yielding AIC_m.

Transaxial images of the brain were reconstructed using filtered backprojection (128×128 matrix, 35 slices, 2.34×2.34× 4.25 mm voxel size). Quantitative parametric maps representing rCBF were calculated using the integration method described by Alpert et al. [5] (see Appendix). The method yields maps of K_1 and k_2, which represent rCBF and rCBF/p respectively (p = partition coefficient).

Compared with the true input curve in the brain (AIC_{true}) the measured time course of arterial activity in the radial artery (AIC_m) is time-shifted and distorted due to dispersion. Both time shift and dispersion were corrected before calculation of the rCBF by the method detailed in the Appendix.

In the volunteer group, maps of rCBF were additionally calculated using Watabe's method ($rCBF_{wat}$) as described in the Appendix. This alternative non-invasive method was then also compared with $rCBF_{K1}$ derived from Alpert's approach.

New method

A summary of the used abbreviations is given in Table 1. The new method is based on washout parameter k_2. Parameter K_1 is directly dependent on the scale of the AIC. If the AIC is multiplied by factor f, K_1 is reduced by $1/f$. In contrast, k_2 is related to the shape and not the scale of the AIC. Furthermore, k_2 is quantitatively related to rCBF ($k2=rCBF/p$, where p is the partition coefficient). The basic idea is to use a standard input curve (AIC_{st}) instead of the measured one to calculate maps of K_{1*} and k_{2*} using Alpert's method (the symbol * is attached to any parameter calculated with the standard input curve). K_{1*} will still reflect the pattern of rCBF, while k_{2*} should quantitatively represent rCBF. An AIC_{st} was constructed by averaging the AIC_m of eight subjects not included in this study. For this purpose each AIC_m was normalised to peak activity and time-shifted to match the peaks. The resulting AIC_{st} is depicted in Fig. 1.

In a second step, $rCBF_{k2*}$ was used to scale $rCBF_{K1*}$. The scaled $rCBF_{K1*}$ maps are denoted $rCBF_{K1*s}$. The reason for producing $rCBF_{K1*s}$ maps is that they are considerably less noisy than $rCBF_{k2*}$ maps. The scaling idea is based on the observation that $rCBF_{K1*}$ maps correctly represent the pattern of rCBF. Following scaling, $rCBF_{K1*}$ is expected to be a quantitative measure for rCBF. The scaling was performed as follows: a template of grey matter voxels was determined by thresholding $rCBF_{K1*}$ at 60% of maximum. The maps of $rCBF_{K1*}$ were then scaled such that the mean of the grey matter voxels equalled the grey matter mean of $rCBF_{k2*}$.

Data analysis

The volunteer data were used to compare the various methods with Alpert's original method and to assess the reproducibility.

Table 1. Summary of abbreviations used

Symbol		Meaning	Units
K_1		rCBF	ml/min/ml$_{tissue}$
rCBF$_{K1}$	$100\,K_1$	Regional CBF	ml/min/100 ml$_{tissue}$
CBF$_{K1}$		Mean of grey matter CBF	ml/min/100 ml$_{tissue}$
p		Partition coefficient	
k_2	K_1/p	Washout rate	min^{-1}
K_{1*}		K_1 calculated with standard input curve	ml/min/ml$_{tissue}$
rCBF$_{K1*}$	$100\,K_{1*}$	Only qualitative map of rCBF	ml/min/100 ml$_{tissue}$
rCBF$_{K1*s}$		rCBF$_{K1*}$ scaled with rCBF$_{k2*}$	ml/min/100 ml$_{tissue}$
k_{2*}		k_2 calculated with standard input curve	min^{-1}
rCBF$_{k2*}$	$100\,k_{2*}$	rCBF based on washout rate	ml/min/100 ml$_{tissue}$
AIC$_m$		Arterial H$_2^{15}$O activity as measured in the external sampling device	kBq/ml
AIC$_{st}$		Standard input curve, mean of 8 AIC$_m$	kBq/ml
AIC$_{true}$		True input curve as seen by the brain	kBq/ml
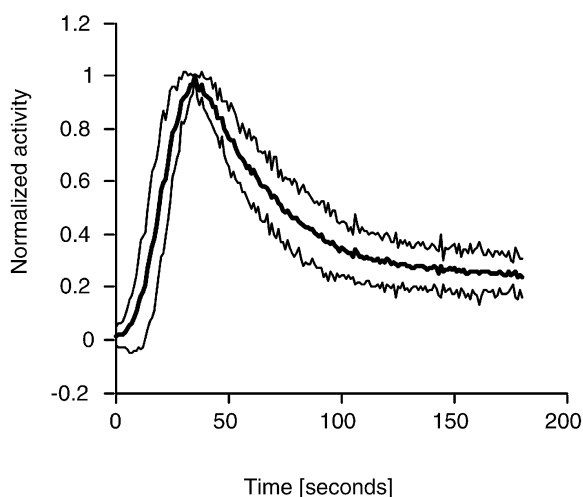
Fig. 1. Input curves. The *middle curve in the top panel* represents the standard input curve used in this study. It was built as the mean of eight individual input curves. The *adjacent lines* are mean±2SD. Before calculating mean and SD, each input curve was normalised to the peak value

The suitability of the methods for the assessment of perfusion reserve was evaluated in the patients.

Volunteers. For the evaluation of the reproducibility the difference scan 3–scan 2 in each session was assessed using Bland-Altman analysis [12]. Bland-Altman plots were furthermore used to compare CBF$_{k2*}$ and CBF$_{wat}$ values with CBF$_{K1}$. The mean values of rCBF$_{K1}$, rCBF$_{k2*}$ and rCBF$_{wat}$ in grey matter were analysed. To determine the latter, all rCBF$_{K1}$ maps were transformed into stereotactic space using SPM99 [13]. The same transformation matrix was then used to spatially normalise the rCBF$_{k2*}$ and rCBF$_{wat}$ maps as well. A template of grey matter voxels was constructed by thresholding the mean of all transformed K_1 maps at 60% of maximum value. This template was then applied to the stereotactically transformed maps of rCBF$_{K1}$, rCBF$_{k2*}$ and rCBF$_{wat}$ to determine the mean values in grey matter, which are denoted as CBF$_{K1}$, CBF$_{k2*}$ and CBF$_{wat}$ respectively.

The method using rCBF$_{K1*s}$ maps was assessed in the same manner. However, since the mean of grey matter voxels had already been used for the scaling, a cerebellar and a white matter region were chosen for the evaluation of reproducibility and the comparison with rCBF$_{K1}$. In addition, statistical parametric mapping (SPM) was performed to evaluate potential region-specific differences in rCBF$_{K1*s}$ and rCBF$_{K1}$. For this purpose all rCBF maps were normalised to the mean of grey matter and smoothed with a 15-mm Gaussian filter. The differences rCBF$_{K1*s}$–rCBF$_{K1}$ and rCBF$_{K1}$–rCBF$_{K1*s}$ were then assessed voxel by voxel using *t* statistic subsequently transformed into normally distributed *z* statistic(SPM99 [13, 14]). Any significant difference (corrected for multiple comparisons) would indicate region-specific deviations from the global difference.

In order to assess the effect of using AICs of varying shapes on CBF$_{k2*}$, one measurement of each volunteer (scan 1 of day 3, arbitrary choice) was fitted with all eight AICs used to construct the AIC$_{st}$.

Patients. An important parameter in the presurgical evaluation of vascular patients is the perfusion reserve (PR), which is the difference between rCBF following acetazolamide and baseline rCBF. In this study, PR is expressed as the percentage increase of rCBF relative to baseline. PR was assessed in a cerebellar region. Cerebellum was chosen because it was devoid of pathology. The PR determined with rCBF$_{k2*}$ and rCBF$_{K1*s}$ was compared to that calculated with rCBF$_{K1}$ using the Bland-Altman method.

Results

The comparison of CBF$_{k2*}$ and CBF$_{wat}$ with the gold standard CBF$_{K1}$ is demonstrated in Fig. 2. CBF$_{k2*}$ was on average 11% higher than CBF$_{K1}$. In contrast, CBF$_{wat}$ was 39% lower. The SD of the difference with CBF$_{K1}$ expressed in percent was also considerably higher for CBF$_{wat}$ than for CBF$_{k2*}$ (23.5% vs 15.6%).

The reproducibility of the various methods is summarised in Fig. 3. The relevant parameter is the SD of the difference CBF$_{scan3}$–CBF$_{scan2}$. Expressed in percent, the value was 6.1% for CBF$_{K1}$ and CBF$_{k2*}$ and 12.0% for CBF$_{wat}$.
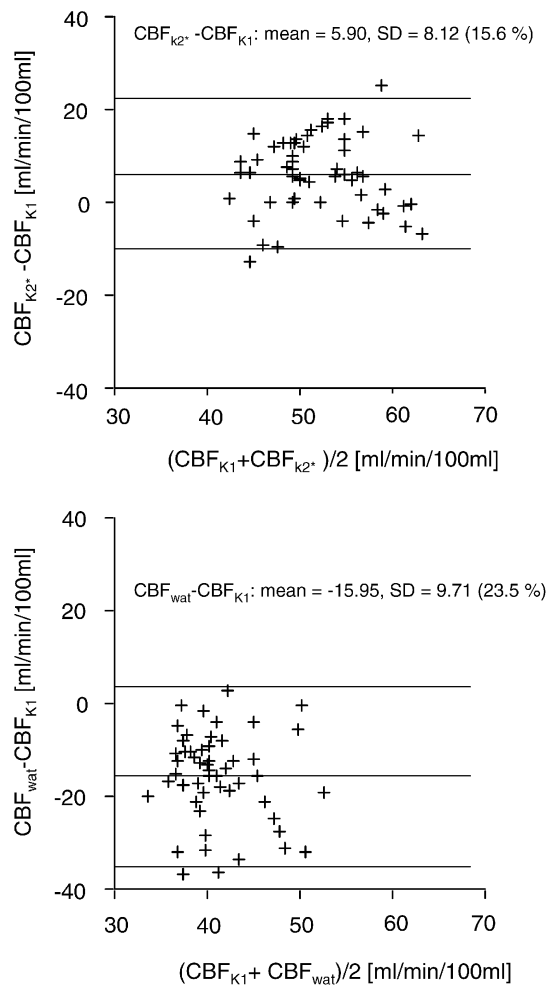
Fig. 2. Bland-Altman plot of the comparison of CBF_{k2*} and CBF_{wat} with CBF_{K1}. The analysis includes a total of 55 scans acquired in ten volunteers. The *middle horizontal line* represents the mean difference, and the *top and bottom lines* are mean±2SD

The variation of CBF_{k2*} with different arterial input curves was determined by calculating CBF_{k2*} of a single PET measurement of each volunteer with all eight AIC_m used to build the standard AIC. The result is presented in Table 2. The coefficient of variation (COV=SD/mean) was chosen as the parameter to indicate the variation. It ranged from 7.8% to 10.9%.

The evaluation of $rCBF_{K1*s}$ in white matter and a cerebellar region is summarised in Fig. 4. In white matter, $rCBF_{K1*s}$ was on average 13.1% higher than $rCBF_{K1}$, and in cerebellum 11.4% higher. In white matter only two of the 55 differences were outside the range mean±2 SD, while in cerebellum only one data point was outside. With regard to reproducibility, the SD of the scan 3–scan 2 differences was 7.3% and 6.5% in white matter and cerebellum respectively. In white matter only one data point was outside the range mean±2 SD, while in cerebellum all data points were inside. Statistical parametric mapping revealed no regions where the local difference
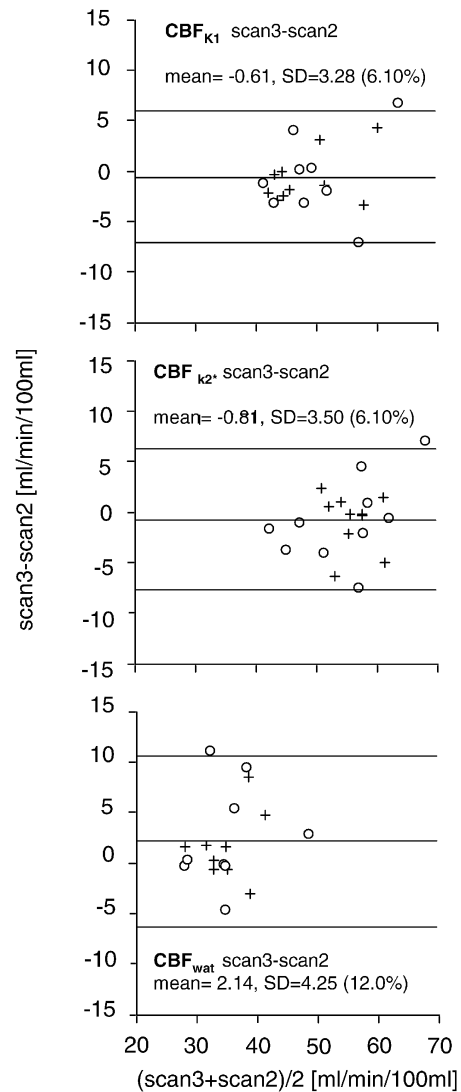
Fig. 3. Bland-Altman plot representing the reproducibility of mean CBF in grey matter for the different methods. The analysis included ten subjects for whom serial measurements 2 days apart were available. The *open circles* represent the values of day 1, and the *crosses* those of day 3. The important parameter for reproducibility is the standard deviation of the scan 3–scan 2 difference, which is indicated together with the mean difference in ml/min/100 ml. The *middle line* represents the mean difference, and the *top and bottom lines* are mean±2SD for the pooled data of day 1 and day 3. The mean and SD are additionally numerically indicated. Mean±SD for day 1 and day 3 separately were as follows: CBF_{K1}: 0.49±4.10 (7.5%), 0.70±2.55 (4.9%); CBF_{k2*}: 0.73±4.22 (7.3%), 0.89±2.81 (5.1%); CBF_{wat}: 2.73±5.10 (14.9%), 1.54±3.37 (8.7%). In parentheses is the SD in percent

between $rCBF_{K1*s}$ and $rCBF_{K1}$ deviated significantly from the global difference.

An example of an acetazolamide study is shown in Fig. 5. It is obvious that the $rCBF_{k2*}$ maps are considerably noisier than the rCBF maps based on K_1.

The comparison of the perfusion reserve determined with $rCBF_{k2*}$, $rCBF_{K1*s}$ and $rCBF_{K1}$ is presented in

Fig. 4. Evaluation of $rCBF_{K1*s}$ in white matter and a cerebellar region. The Bland-Altman plot of the comparison $rCBF_{K1*s}$ with $rCBF_{K1}$ is shown in the *top two panels* (pooled data, 55 measurements). The Bland-Altman plot of the reproducibility as assessed by the scan 3–scan 2 difference is demonstrated in the *bottom panels*. *Open circles* represent the data of day 1, and *crosses* those of day 3. The indicated numbers are for the pooled data

white matter

$rCBF_{K1*s}$-CBF_{K1}
mean = 3.44, SD = 3.95 (14.6 %)

scan3-scan2
mean = -0.71, SD = 2.17 (7.3 %)

cerebellum

$rCBF_{K1*s}$-CBF_{K1}
mean = 5.75, SD = 8.02 (15.9 %)

scan3-scan2
mean = -1.49, SD = 3.33 (6.5 %)

($rCBF_{K1*s}$ + $rCBF_{K1}$)/2 [ml/min/100ml]

(scan + scan2)/2 [ml/min/100ml]
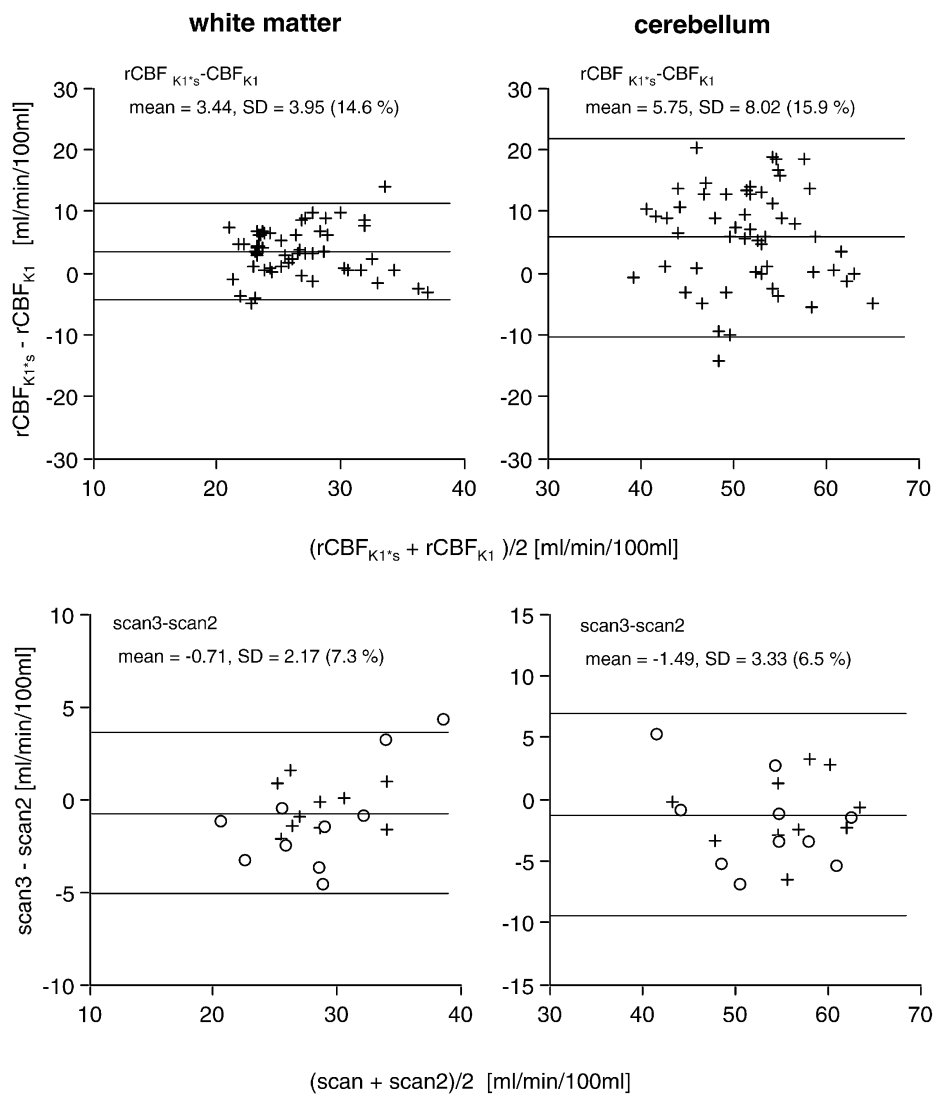
Table 2. $rCBF_{k2}$ and coefficient of variation calculated with the eight input curves used to derive the mean input curve

Volunteer	Mean $rCBF_{k2}$ (ml/min/100 g)	COV (%)
1	59.02	7.8
2	55.47	10.5
3	56.37	10.6
4	60.93	10.4
5	62.41	9.5
6	55.69	8.1
7	60.46	10.0
8	64.89	9.6
9	60.96	10.9
10	64.21	10.0
Mean	60.04	9.7

Fig. 6. On average, PR_{k2*} was 6.5% lower than PR_{K1}, while PR_{K1*s} was similar to PR_{K1} (top panels). The correlation of PR_{k2*} and PR_{K1*s} with PR_{K1} was excellent (bottom panels). The indicated numbers refer to PR expressed in percentage increase from baseline. The values were also calculated for PR in ml/min/100 ml. In these units the difference PR_{k2*}–PR_{K1} was 5.16±6.88, and the difference PR_{K1*s}–PR_{K1} was 3.19±7.95.

Discussion

$H_2^{15}O$ is a diffusible, inert tracer. Its kinetics following intravenous injection is determined by two main parameters. The washin rate K_1 corresponds to rCBF and the washout rate k_2 is rCBF divided by the partition coefficient. From a more mathematical point of view, Eq. 2 in the Appendix demonstrates that K_1 is a scale factor, while k_2 determines the shape of the tissue time-activity curve (TAC). In cases where the arterial input curve is a

Fig. 5. Example of an acetazolamide examination of a patient with a right internal carotid artery stenosis. The images represent a slice at the level of the basal ganglia. The perfusion reserve is clearly impaired in the territory of the right middle cerebral artery. This is obvious on the maps of rCBF$_{K1}$ and rCBF$_{K1scaled}$, but can only be guessed on the rCBF$_{k2*}$ map
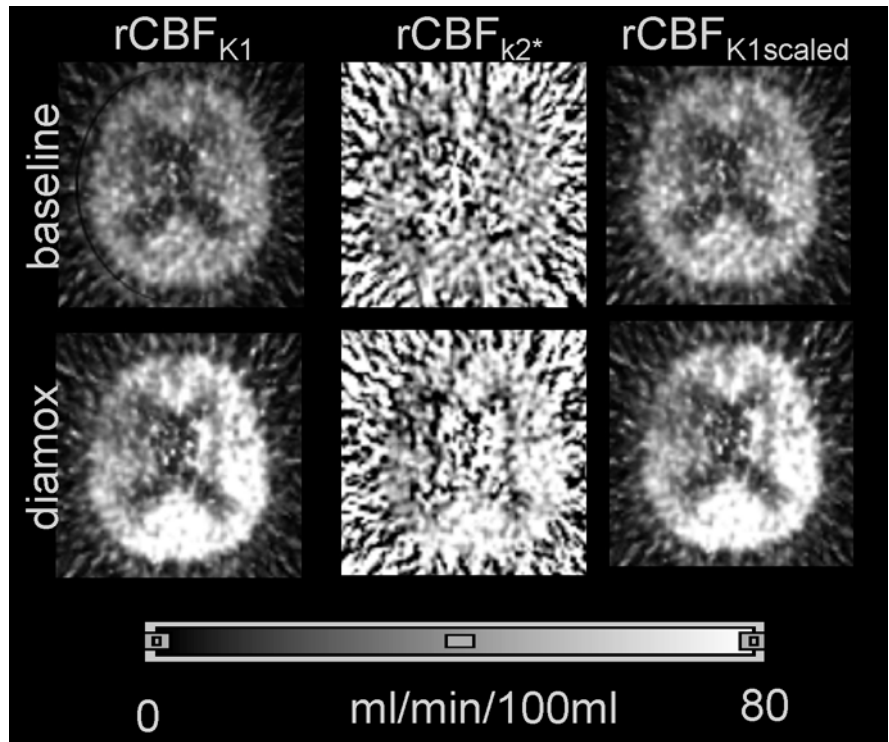
Fig. 6. Comparison of the perfusion reserve determined with rCBF$_{K1}$, rCBF$_{k2*}$ and rCBF$_{K1*s}$. The *top two panels* represent the Bland-Altman plot, and the *bottom plots* show the linear regression; r is Pearson's correlation coefficient. On the *left* is the comparison of PR determined with rCBF$_{k2*}$ and rCBF$_{K1}$; on the *right* is the comparison of PR calculated with rCBF$_{K1*s}$ and rCBF$_{K1}$
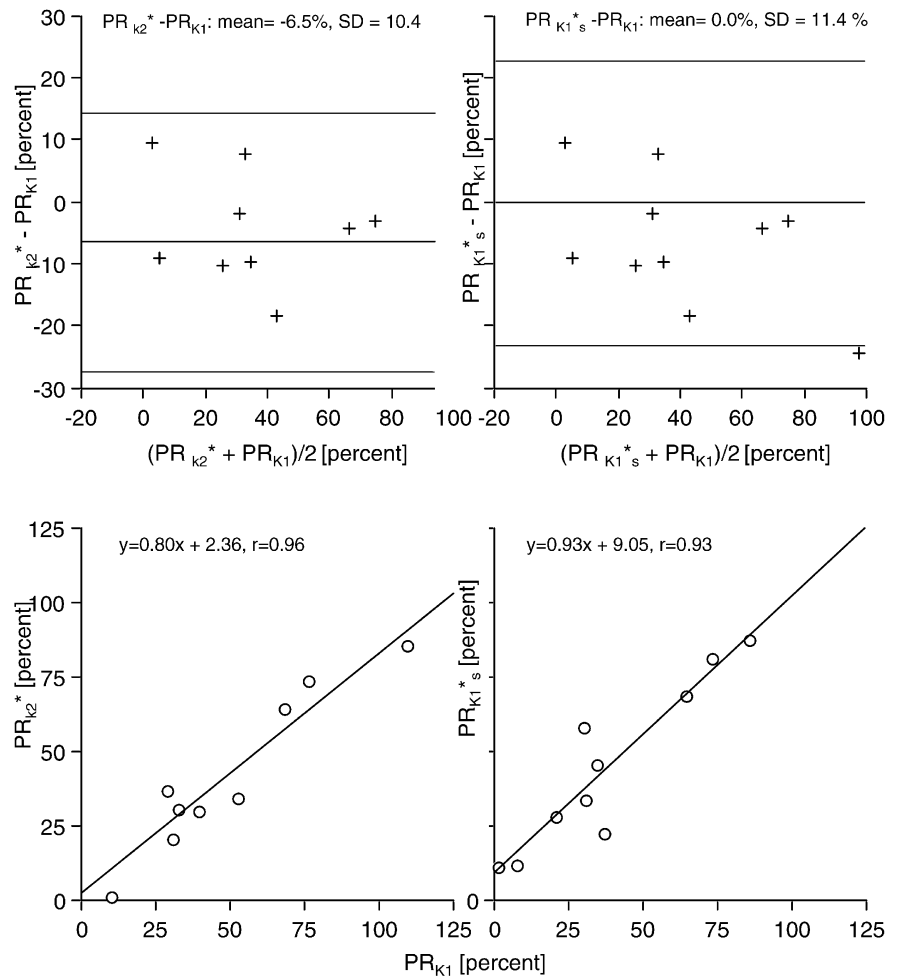
short spike, the TAC would be described by a decaying mono-exponential. This situation can be realised with an intra-arterial injection, as is possible in experimental settings [15]. rCBF can then be easily determined by fitting a mono-exponential to the TACs. With an intravenous injection the input curve, and with it the TAC, become dispersed. This is why some type of input curve is needed to extract $rCBF_{k2*}$ in the presented method. The degree of dispersion is dependent on the shape of the input curve. It is clear that $rCBF_{K1*}$ calculated with the standard input curve is not scaled properly. However, $rCBF_{k2*}$ reflects rCBF in a quantitative manner, as is demonstrated in this work. It is probably advantageous to use a standardised injection protocol using an automated device which results in very similar input curves within the same subject, but also among subjects. Thus the shape of the standard input curve, which is built from an ensemble of eight individual input curves, can be expected to be a reasonable approximation of the measured $H_2^{15}O$ activity in the sampling device. It is important to keep in mind that the input curves (measured or standard) used to calculate rCBF values are corrected for dispersion and delay before the calculation of rCBF maps. This likely explains why the $rCBF_{k2*}$ maps of one individual measurement evaluated with the eight different input curves show relatively little variation as estimated by the coefficient of variation (Table 2, mean COV=9.7%). There seems to be enough flexibility in the correction for dispersion to retrieve the shape of the true input curve AIC_{true} from the standard curve AIC_{st}. It is not clear how well the used standard input curve would work if the actual input curve were to deviate substantially, for instance with manual tracer injection. It seems reasonable to suggest that each centre creates its own standard input curve.

Figure 2 demonstrates that CBF_{k2*} is on average 5.9 ml/min/100 ml higher than CBF_{K1}, corresponding to an 11% difference. This is an expected result since k_2 is K_1/p and the partition coefficient p is smaller than 1. In fact, the 11% difference corresponds to a p of 0.89, which is in line with previously reported values [16]. In principle one could remove this bias by multiplying $rCBF_{k2*}$ by 0.89. All but two data points are contained within the range defined by mean±2SD, indicating a good agreement between $rCBF_{k2*}$ and $rCBF_{K1}$.

The reproducibility in the range of 6.1–7.3% for CBF_{K1}, CBF_{k2*} and $rCBF_{K1*s}$ is in line with previously published data. Matthew et al. performed two serial $H_2^{15}O$ scans in 25 human subjects and reported a reproducibility of whole brain blood flow measurements of 8.7% [17]. In another study involving seven monkeys, the standard deviation of the difference of two successive measurements was 11% [18]. In this study it was 6.1% for CBF_{K1} and CBF_{k2*}, but considerably worse for the Watabe approach (12%).

In our comparisons the Watabe approach yielded considerably lower values for CBF than Alpert's method, which is in contrast to the originally published data [8]. The reason is not clear. It was observed in this work that the method critically depended on the choice of the starting values. This may explain some of the discrepancy with the previously reported results. In addition, the reproducibility was remarkably worse for Watabe's approach compared with the newly evaluated method.

As demonstrated in Fig. 5, it is obvious that the images of $rCBF_{k2*}$ are much noisier than maps based on K_1. They are therefore not suited to evaluate changes in small areas. An easy solution is to use the $rCBF_{k2*}$ values to scale $rCBF_{K1*}$ maps, which are of much higher statistical quality.

The final product of the presented method are the $rCBF_{K1*s}$ maps. Their evaluation of is summarised in Fig. 4. Since $rCBF_{K1*s}$ maps were scaled with the grey matter average, the evaluation was performed in two regions outside the grey matter template used for the scaling, namely white matter and cerebellum. The results are in line with that described for CBF_{k2*}. There was high agreement between $rCBF_{K1*s}$ and $rCBF_{K1}$ in both regions. Again, $rCBF_{K1*s}$ was between 11% and 13% higher than $rCBF_{K1}$, corresponding to a partition coefficient of 0.87–0.89. As mentioned before, this bias could be removed by considering p in the scaling of $rCBF_{K1*}$. However, a potential problem may arise if the partition coefficient in the area used for scaling substantially deviates from normal. The reproducibility of $rCBF_{K1*s}$ was high, in the same range as for $rCBF_{k2*}$ and $rCBF_{K1}$. The validity of using $rCBF_{K1*s}$ maps is further supported by Fig. 6. The Bland-Altman plot of the comparison of the PR derived from $rCBF_{K1*s}$ and $rCBF_{k2*}$ with the PR derived from $rCBF_{K1}$ demonstrates a high agreement. Another issue is whether there might be areas where the local difference between $rCBF_{K1*s}$ and $rCBF_{K1}$ deviates from the global difference. Statistical parametric mapping revealed no such areas. In general it is noted that the flow values in grey matter are relatively low and in white matter relatively high. This is likely due to the limited resolution of the PET scanner. In principle there exist algorithms to correct for this bias [19]. However, these are as yet not widely used in clinical settings.

In conclusion, a new non-invasive method for the quantitative determination of rCBF is presented. The method is in good agreement with Alpert's original method and reproducibility is high. It does not require arterial blood sampling, yields quantitative voxel-by-voxel maps of rCBF, and is computationally efficient and easy to implement.

Appendix

Quantitative parametric maps representing regional cerebral blood flow (rCBF) were calculated using the time-weighted integral method described by Alpert et al. [5] and a method not requiring arterial blood data described by Watabe et al. [8]. Both are based on the one-tissue compartment model for $H_2^{15}O$ represented by the differential equation:

$$\frac{dC(t)}{dt} = K_1 C_a(t) - k_2 C(t) \tag{1}$$

where $C(t)$ denotes tissue activity concentration, $C_a(t)$ the measured arterial input function (AIF), K_1=rCBF and k_2=rCBF/p (flow/partition coefficient). Assuming no tissue activity before tracer application at time zero, the solution of Eq. 1 is given by:

$$C(t) = K_1 C_a(t) \otimes e^{-k_2 t} = K_1 \int_0^t C_a(u) e^{k_2(u-t)} du \tag{2}$$

Alpert's method represents a computationally efficient implementation of the flow calculations based on the time course of the activity concentration in each voxel and the AIF.

Essentially, a lookup table r is calculated from the blood data as follows:

$$r = \frac{\int_0^T \int_0^t C_a(u) e^{k_2(u-t)} du\, dt}{\int_0^T t \int_0^t C_a(u) e^{k_2(u-t)} du\, dt} \tag{3}$$

where T denotes the acquisition duration, and k_2 is varied in 400 increments between 0 and 200 (ml/min/100 g tissue) to cover the range of k_2 occurring in physiological conditions. A similar operation is performed with the PET data in each voxel:

$$\hat{r} = \frac{\int_0^T C(u) du\, dt}{\int_0^T t C(u) du\, dt} \tag{4}$$

From $\hat{r}$, the actual k_2 is obtained by a lookup in the r table. The flow is finally calculated by entering k_2 into the equation:

$$rCBF = K1 = \frac{\int_0^T C(u) du\, dt}{\int_0^T t \int_0^t C_a(u) e^{k_2(u-t)} du\, dt} \tag{5}$$

Compared with the true input curve in the brain, the measured time course of arterial activity in the radial artery is time-shifted and distorted due to dispersion. Both time shift and dispersion were corrected before rCBF calculation by the method described by Meyer [20]. To this end, a flow model including the delay and an expo-

nential dispersion as parameters was fitted to the averaged time-activity curve of all brain voxels with integrated activity above 40% of the maximum. The measured AIF was then shifted by the estimated delay, and deconvolved by the exponentially decaying dispersion using a Fourier transform approach.

Watabe's method uses a reference tissue approach. Equation 1 is integrated twice for the tissue of interest $C(t)$, yielding:

$$\int_0^T C(t) dt = K_1 \int_0^T \int_0^t C_a(u) du\, dt - \frac{K_1}{p} \int_0^T \int_0^t C(u) du\, dt \tag{6}$$

The same operation is performed for a reference tissue $C^{Ref}(t)$. From the two resulting expressions $C_a(t)$ can be algebraically eliminated, yielding equation:

$$\int_0^T C^{Ref}(t) dt = \frac{K_1^{Ref}}{K_1} \int_0^T C(u) dt + \frac{K_1^{Ref}}{p} \int_0^T \int_0^t C(u) du\, dt$$
$$- \frac{K_1^{Ref}}{p^{Ref}} \int_0^T \int_0^t C^{Ref}(u) du\, dt \tag{7}$$

which contains the tracer concentration in the two tissue regions as measured quantities and the flows (K_1, K_1^{Ref}), and partition coefficients (p, p^{Ref}) as the unknowns. This equation can be solved for K_1:

$$rCBF = K_1$$

$$= \frac{\int_0^T C(t) dt}{\frac{1}{K_1^{Ref}} \int_0^T C^{Ref}(t) dt + \frac{1}{p^{Ref}} \int_0^T \int_0^t C^{Ref}(u) du\, dt - \frac{1}{p} \int_0^T \int_0^t C(u) du\, dt} \tag{8}$$

In an initial pre-processing step, time-activity curves were calculated for two clusters of brain voxels: the "low-flow" voxels defined as the 5,000 voxels with the lowest integrated activity [$C(t)$], and the "high-flow" voxels, serving as the reference and defined as the 2,000 voxels with the highest integrated activity [$C^{Ref}(t)$]. Equation 7 evaluated at all acquisition times ($T=T_i$, i=1...18) then served as the operational equation from which the unknowns (K_1, K_1^{Ref}, p, p^{Ref}) were estimated in an iterative optimisation using a Marquardt-Levenberg algorithm. Subsequently, Eq. 8 was applied to calculate flow for all voxel-wise time-activity curves $C(t)$ in a single step. Hereby, a fixed partition coefficient p=0.86 ml/ml [16] was assumed, and K_1^{Ref} and p^{Ref} resulting from pre-processing were inserted.

The pre-processing step is crucial for the results of the flow calculations. As four parameters are estimated in a fit to a smooth curve, a dependency of the results on the starting parameters was noted, indicating that the method is prone to local minima. Therefore the flow and the partition coefficient were determined for the time-activity

curves of the low-flow and the high-flow voxel clusters in one volunteer study by means of a full one-tissue compartment model analysis using the AIF. The result parameters were then used as a standard set of starting parameters for K_1, K_1^{Ref}, p and p^{Ref} (13, 63, 0.3 and 1.0 respectively).

All computations were performed with the dedicated software PMOD (www.pmod.com) [21]. This JAVA-based software allows the easy implementation of the necessary models to calculate rCBF, including the corrections of the input curve.

References

1. Kuwabara Y, Ichiya Y, Sasaki M, Yoshida T, Masuda K. Time dependency of the acetazolamide effect on cerebral hemodynamics in patients with chronic occlusive cerebral arteries. Early steal phenomenon demonstrated by [^{15}O]H$_2$O positron emission tomography. Stroke 1995; 26:1825–1829.

2. Ramsay SC, Yeates MG, Lord RS, Hille N, Yeates P, Eberl S, Reid C, Fernandes V. Use of technetium-HMPAO to demonstrate changes in cerebral blood flow reserve following carotid endarterectomy. J Nucl Med 1991; 32:1382–1386.

3. Schmiedek P, Piepgras A, Leinsinger G, Kirsch CM, Einhupl K. Improvement of cerebrovascular reserve capacity by EC-IC arterial bypass surgery in patients with ICA occlusion and hemodynamic cerebral ischemia. J Neurosurg 1994; 81:236–244.

4. Vorstrup S, Brun B, Lassen NA. Evaluation of the cerebral vasodilatory capacity by the acetazolamide test before EC-IC bypass surgery in patients with occlusion of the internal carotid artery. Stroke 1986; 17:1291–1298.

5. Alpert NM, Eriksson L, Chang JY, Bergstrom M, Litton JE, Correia JA, Bohm C, Ackerman RH, Taveras JM. Strategy for the measurement of regional cerebral blood flow using short-lived tracers and emission tomography. J Cereb Blood Flow Metab 1984; 4:28–34.

6. Kanno I, Lammertsma AA, Heather JD, Gibbs JM, Rhodes CG, Clark JC, Jones T. Measurement of cerebral blood flow using bolus inhalation of C^{15}O$_2$ and positron emission tomography: description of the method and its comparison with the C^{15}O$_2$ continuous inhalation method. J Cereb Blood Flow Metab 1984; 4:224–234.

7. Raichle ME, Martin WR, Herscovitch P, Mintun MA, Markham J. Brain blood flow measured with intravenous H$_2$^{15}O. II. Implementation and validation. J Nucl Med 1983; 24:790–798.

8. Watabe H, Itoh M, Cunningham V, Lammertsma AA, Bloomfield P, Mejia M, Fujiwara T, Jones AK, Jones T, Nakamura T. Noninvasive quantification of rCBF using positron emission tomography. J Cereb Blood Flow Metab 1996; 16:311–319.

9. Fox PT, Mintun MA, Raichle ME, Herscovitch P. A noninvasive approach to quantitative functional brain mapping with H$_2$^{15}O and positron emission tomography. J Cereb Blood Flow Metab 1984; 4:329–333.

10. Arigoni M, Kneifel S, Fandino J, Khan N, Burger C, Buck A. Simplified quantitative determination of cerebral perfusion reserve with H$_2$^{15}O PET and acetazolamide. Eur J Nucl Med 2000; 27:1557–1563.

11. Suzuki J, Takaku A. Cerebrovascular "moyamoya" disease. Disease showing abnormal net-like vessels in base of brain. Arch Neurol 1969; 20:288–299.

12. Bland JM, Altman DG. Statistical methods for assessing agreement between two methods of clinical measurement. Lancet 1986; 1:307–310.

13. Friston KJ, Ashburner J, Poline JB, Frith CD, Heather JD, Frackowiak RSJ. Spatial registration and normalisation of images. Human Brain Mapping 1995; 2:165–189.

14. Friston KJ, Holmes AP, Worsley KJ, Poline JB, Frith CD, Frackowiak RSJ. Statistical parametric maps in functional imaging: a general linear approach. Human Brain Mapping 1995; 2:189–210.

15. Buck A, Mulholland GK, Papadopoulos SM, Koeppe RA, Frey KA. Kinetic evaluation of positron-emitting muscarinic receptor ligands employing direct intracarotid injection. J Cereb Blood Flow Metab 1996; 16:1280–1287.

16. Lammertsma AA, Martin AJ, Friston KJ, Jones T. In vivo measurement of the volume of distribution of water in cerebral grey matter: effects on the calculation of regional cerebral blood flow. J Cereb Blood Flow Metab 1992; 12:291–295.

17. Matthew E, Andreason P, Carson RE, Herscovitch P, Pettigrew K, Cohen R, King C, Johanson CE, Paul SM. Reproducibility of resting cerebral blood flow measurements with H$_2$^{15}O positron emission tomography in humans. J Cereb Blood Flow Metab 1993; 13:748–754.

18. Iida H, Law I, Pakkenberg B, Krarup-Hansen A, Eberl S, Holm S, Hansen AK, Gundersen HJ, Thomsen C, Svarer C, Ring P, Friberg L, Paulson OB. Quantitation of regional cerebral blood flow corrected for partial volume effect using O-15 water and PET. I. Theory, error analysis, and stereologic comparison. J Cereb Blood Flow Metab 2000; 20:1237–1251.

19. Law I, Iida H, Holm S, Nour S, Rostrup E, Svarer C, Paulson OB. Quantitation of regional cerebral blood flow corrected for partial volume effect using O-15 water and PET. II. Normal values and gray matter blood flow response to visual activation. J Cereb Blood Flow Metab 2000; 20:1252–1263.

20. Meyer E. Simultaneous correction for tracer arrival delay and dispersion in CBF measurements by the H$_2$^{15}O autoradiographic method and dynamic PET. J Nucl Med 1989; 30:1069–1078.

21. Mikolajczyk K, Szabatin M, Rudnicki P, Grodzki M, Burger C. A JAVA environment for medical image data analysis: initial application for brain PET quantitation. Med Inform (Lond) 1998; 23:207–214.